Generation of vorticity at the open end of acoustic waveguides

León Martínez del Río

*Instituto de Ciencias Aplicadas y Tecnología, Universidad Nacional Autónoma de México, Circuito Exterior,
Ciudad Universitaria, Mexico City 04510, Mexico*

Carlos Málaga ⬤

*Facultad de Ciencias, Universidad Nacional Autónoma de México, Circuito Exterior, Ciudad Universitaria,
Mexico City 04510, Mexico*

Roberto Zenit

School of Engineering, Brown University, 184 Hope St., Providence, Rhode Island 02912, United States

Pablo L. Rendón ⬤[*]

*Instituto de Ciencias Aplicadas y Tecnología, Universidad Nacional Autónoma de México, Circuito Exterior,
Ciudad Universitaria, Mexico City 04510, Mexico*

For periodic acoustic fields of sufficient intensity inside a cylindrical tube, a nonlinear mechanism is responsible for the generation of vorticity at the open end of the tube. It has been observed that as the magnitude of the acoustic velocity is increased, different regimes are possible. At first, we consider the inner edge of the duct to be straight. In the first regime, vorticity appears only in the immediate vicinity of the open end of the tube. For higher acoustic velocities, vortex rings are formed at this same location, and finally, for even larger velocities, they are advected outwards. In all cases roundingoff the inner edge of the tube to different degrees leads to a suppression of the mechanism responsible for the generation of vorticity, with the more noticeable suppression occurring for the smoother edges. The parameter that determines the scale at which different behaviors occur is a Reynolds number R_δ associated with the width of the acoustic boundary layer inside the duct. We use a three-dimensional Lattice Boltzmann Method (LBM) to simulate the velocity and the pressure fields at the exit of the tube, for different values of R_δ, allowing for validation of the numerical method against experimental measurements. In this regard, we conduct experiments with 2D phase-locked particle image velocimetry (PL-PIV) within a similar range of values of R_δ. The expected behavior is observed in both experimental and numerical results, and the results obtained by means of the numerical scheme are consistent with those obtained through PIV measurements, with different regimes exhibiting varying combinations of acoustic streaming, boundary-layer separation, and vortex shedding.

I. INTRODUCTION

The oscillation of high-amplitude acoustic waves near the lowest resonant frequency in a cylindrical tube filled with air is known to produce a variety of nonlinear phenomena at the open end of the tube, such as radiation of shock waves, acoustic streaming, and vortex formation and

---

[*]Corresponding author: pablo.rendon@icat.unam.mx

shedding. The appearance of these structures is accompanied by nonlinear losses, which have been studied extensively both at the open ends of tubes and at orifices along their sides [1–3]. It has been shown, however, that the scale of these losses depends critically on the geometry of the inner edge of the open end of the tube [4]. The coupling between high-intensity acoustic standing waves in a duct and vortex generation at open ends or orifices is relevant in the context of flow distribution systems such as those used to distribute gas at high pressures [4] and sound production in musical wind instruments [5]. For orifices, it has been observed that the nonlinear response of the flow patterns at the orifice openings depends on the acoustic particle velocity, the frequency of oscillation, and the diameter and thickness of the orifices [1]. It is possible to distinguish different regimes, starting with generation of vorticity close to the orifice opening for moderate velocities, and eventually the formation of jets accompanied by formation and shedding of vortex rings for larger velocities. Since the flow patterns at the open end of a long, narrow duct resemble those at an orifice opening [1,3] we assume the general behavior and transition to different regimes are also determined by the values of the acoustic particle velocity, the oscillation frequency, and the diameter of the tube. However, the behavior of the velocity field at the open end of the tube is determined by the competing effects of nonlinear steepening and thermoviscous dissipation in the main wave and the boundary layers which form against the walls, so that we must also take into account the effect of viscosity. In general terms, two nonlinear regimes have been identified at the open end of a long, narrow duct with sharp inner edges, and they depend mostly on the amplitude of excitation of the acoustic field in the tube. In the first regime, when the acoustic velocity is large enough, vorticity appears in the immediate vicinity of the tube. In the second regime, for even larger velocities, vortex rings are formed at the open end of the tube and are advected outwards [3]. Disselhorst and Van Wijngaarden [6] observed that in this case a jet is formed at the mouth of the tube during outflow and boundary-layer separation occurs during inflow. As the acoustic cycle progresses, vortices formed during inflow are advected outwards by the jet, which is in turn fed by air drawn in from the sides of the tube opening. It has also been observed, however, that for rounded edges at equivalent amplitudes of the acoustic field, the formation of vortices at the edge of the open end of the tube is suppressed [3,6]. See Fig. 1 for an illustration of these phenomena.

Apart from the effects discussed above, the flow is expected to show some turbulentlike features at the edges of the open duct due to the large particle velocities. For large oscillation amplitudes in piston-driven resonance tubes, a variety of authors have reported observing turbulence in the boundary layer [7,8]. It is generally agreed that if the tubes have radius a, then the transition to turbulence is a local event provided the dimensionless parameter $\delta/a \ll 1$, where δ is the width of the Stokes boundary layer. For an oscillation with angular frequency ω in a medium with kinematic viscosity ν, we have $\delta = (2\nu/\omega)^{1/2}$. The transition to turbulence is then governed by a local Reynolds number, Re_δ, based on the acoustic boundary layer thickness:

$$R_\delta = \frac{\delta U}{\nu} = \frac{2^{\frac{1}{2}} U}{\sqrt{\omega \nu}}, \tag{1}$$

where U is the mean velocity amplitude. For oscillatory flow, Peube [9] has identified $R_\delta = 22$ as a threshold value above which acoustic streaming may occur. A similar threshold value of Re_δ for the onset of turbulence in similar conditions is not available as values given by different authors vary widely [10,11]. Even if turbulence does occur, however, Merkli and Thomann [7] proved that turbulence will not occur during the whole cycle, and the appearance of turbulence is always followed by relaminarization. In the system under study, the appearance of turbulence accompanies the formation of vortical structures, and thus, the parameter Re_δ is a good indicator to use to mark the transition between regimes.

In this study we aim to observe the transitions between regimes related to particle velocity at the exit of the open end of a cylindrical tube. For this purpose we used particle image velocimetry (PIV) to visualize flow at the exit of the open end of the tube, in combination with three-dimensional numerical simulations using the Lattice Boltzmann method (LBM). The Lattice Boltzmann method
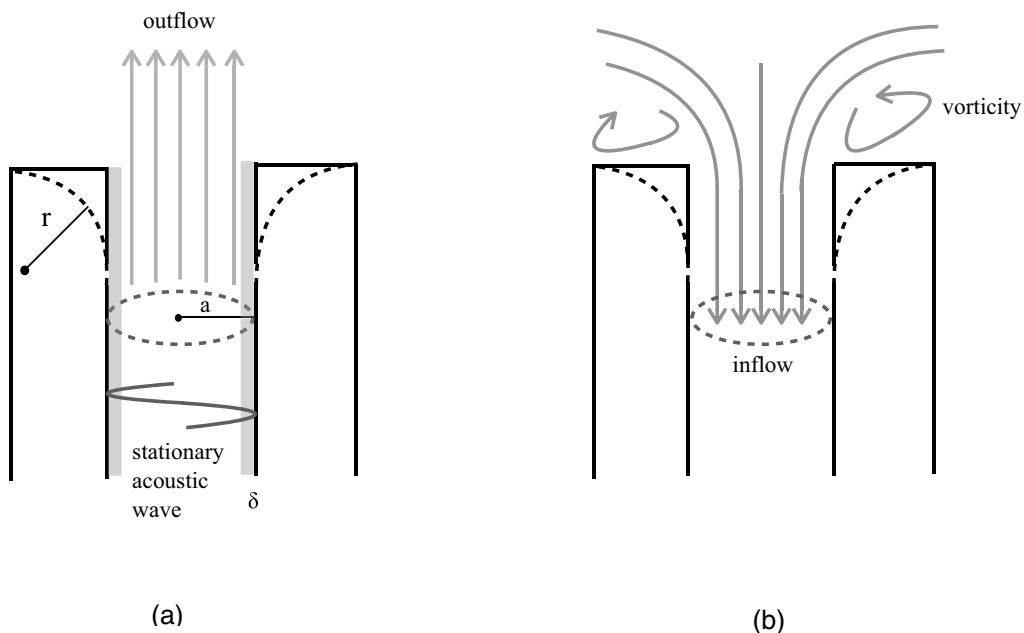
FIG. 1. (a) Outflow and (b) inflow at the open end of a duct with straight (solid line) or rounded edges corresponding to $r > 0$ (dotted line). The radius of the duct is a and the width of the Stokes boundary layer is δ. During inflow vorticity is generated at the inner edges of the duct, especially for $r \ll 1$.

is suitable in this context because it approximates solutions to weakly compressible viscous flow for low Mach numbers, and it can be expected to portray adequately the phenomenon of boundary layer separation. Three-dimensional simulations are necessary in this context, not only because they allow for validation against experimental measurements, which is not possible for two-dimensional simulations [3], but also because nonaxisymmetric instabilities may occur as the intensity of the acoustic field increases and mean flow develops in the pipe [12]. For high particle velocities, we found that both a central jet and vortex rings form around the edges of the open end of the tube, and small-scale perturbations appear in the PIV portrait of the velocity field that propagate from the outer edges of the duct outwards. The behavior at the end of the open pipe depends on the interplay between nonlinearity, viscosity, and the geometry of the open end. A comprehensive study of the manner in which these phenomena combine in a three-dimensional domain to give rise, or not, to boundary layer separation at the open end and, further, to shedding of vortices, is necessary if one is to be able to control these effects. The introduction of horns at the tube exit, for example, has been shown to greatly affect the aeroacoustic behavior at the open end termination [4].

II. PARTICLE IMAGE VELOCIMETRY MEASUREMENTS

Particle image velocimetry (PIV) is a nonintrusive optical technique for the visualization of fluid flow which also allows for the instantaneous measurement of the fluid velocity. Although this technique is most commonly used for liquids, it has also been applied successfully in the field of aeroacoustics for measurements of oscillatory flows in air [3,13–15] and acoustic streaming [16]. The basic principle of two-dimensional PIV consists of seeding the fluid with tracer particles which are both small and light enough to follow the flow. The positions of these particles within a plane
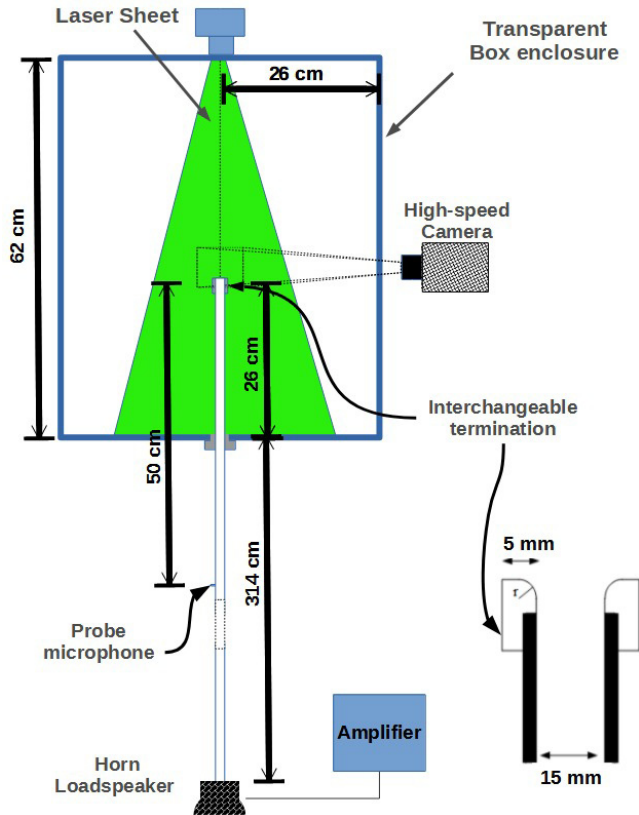
FIG. 2. Experimental configuration.

at a given instant are then captured by a high-speed digital camera when they are illuminated by a thin pulsed laser sheet. The velocity can be obtained by measuring the displacement of the clusters of particles over the time elapsed between frames, typically using a cross-correlation statistical method for this purpose. The relatively rare usage of PIV in air is due to the difficulties which arise from the possibility of weight and buoyancy forces affecting the dynamics of the seeding particles. For the problem at hand, we have set up a PIV system capable of measuring two-dimensional velocity fields in air over short periods of time, and it is described in the following subsection. Several good references exist which give wide overviews of the method, for both liquids and air [17–20], with the paper by Weyna and Mickiewicz [21] being particularly relevant because of its use of phaselocking to analyze periodic signals in air. We also make use of this technique, which involves careful synchronization of the periodic acoustic signal with the image acquisition process in order to obtain image pairs corresponding to equal phases within different cycles, which are then transformed to vector fields and averaged to determine the instantaneous velocity vector field.

A. Experimental setup

The main features of the experimental setup are shown in Fig. 2. The volume to be studied was located at the open end of a cylindrical tube within which an intense acoustic field was generated. The acoustic field inside the tube was generated by an Eighteen HD2080T horn loudspeaker, driven by a Yamaha P2500S amplifier, and coupled to the tube by means of a custom-made adapter. The signal fed to the amplifier was a 50 Hz sine wave synthesized with Matlab and generated
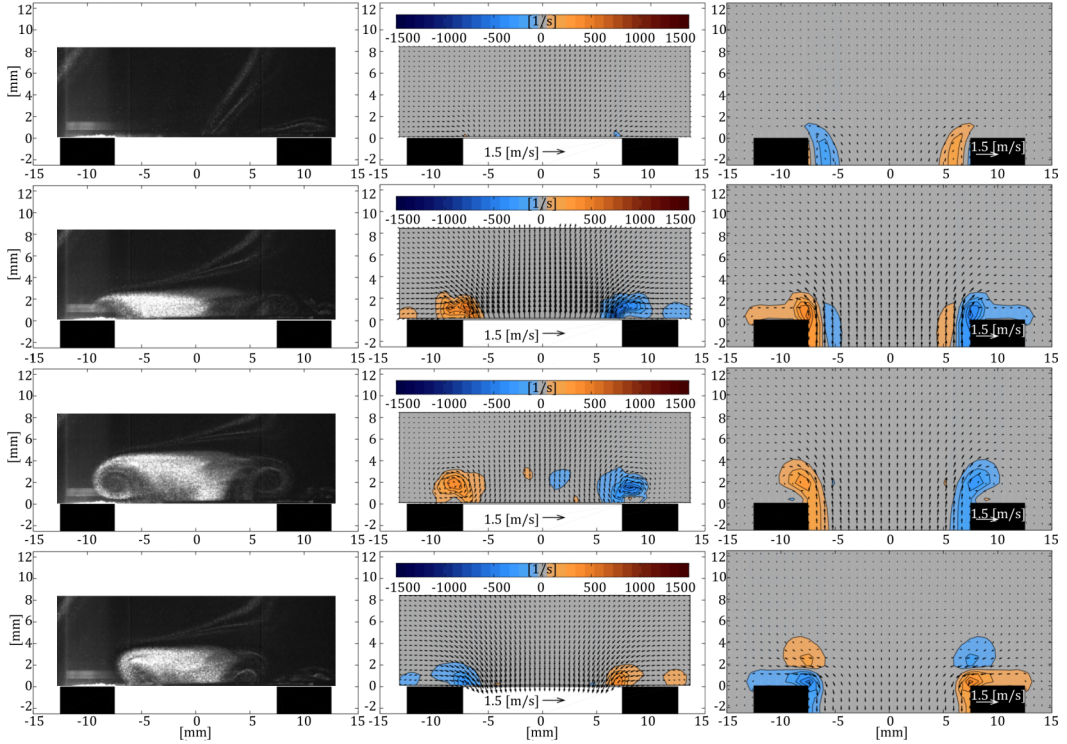
FIG. 3. Nonlinear response at the open end of the duct with $R_\delta = 20.2$ and $r = 0$ mm, illustrating the generation of vorticity at the inner edge of the tube. Images of the tracing particles are displayed in the left column, the velocity field and the azimuthal component of vorticity field $[1/s]$ obtained by means of PIV are shown in the center column, with the corresponding axial slices of the scaled velocity field and azimuthal component of the vorticity field $[1/s]$ resulting from LBM simulations plotted in the right column. Successive phases correspond to different rows: (a) $0.0\,T$, (b) $0.3\,T$, (c) $0.5\,T$, and (d) $0.7\,T$, where T is the oscillation period.

by a Tascam 144MK II audio interface. The tube itself was 3.40 m long with an internal diameter measuring 15 mm, so that the frequency of the first resonance was 50 Hz. The acoustic pressure inside the tube was measured using a Brüel and Kjaer type 4182 sound pressure probe microphone inserted into tube through a narrow hole drilled at a distance of 50 cm from the open end of the tube. Four interchangeable tube terminations at the open end were available with edges rounded, or chamfered, to different degrees, characterized by the radii of curvature r at the edges: $r = 0$ mm for the straight-edge, and $r = 1.7$ mm, $r = 3.4$ mm, $r = 5.0$ mm for the three rounded edges. In order to contain the seeding particles, the open-end termination was placed inside a sealed box made of acrylic in the shape of an octagonal prism, with a height of 60 cm and a side length of 21 cm. The open end of the tube is located at a distance of 26 cm from the internal base of the box. The seeding particles themselves consisted of oil droplets with a mean diameter of $1\,\mu$m produced by a Dantec fog generator and left to homogenize in the box for 10 minutes before each experiment, with no significant movement of the particles detected due to gravity during this span of time.

Illumination of the particle tracers was achieved using a dual-cavity flash-pumped Nd:YLF laser with light sheet optics. The light sheet was aligned with the axis of the tube, and a Phantom SenseSpeed 9000 high-speed camera was then positioned perpendicular to the light sheet. For each measurement, two images were captured by the camera. A Dantec model 523 BNC synchronizer

was used for the frame straddling. The two images were separated by 0.2 ms and in both cases exposition time was 0.02 ms. The PIV analysis was carried out using cross-correlation between the images with a search area of 32×32 pixels with an overlap of 50%. A three-point Gaussian fit [19] was applied with a local median filter.

III. LATTICE BOLTZMANN NUMERICAL SIMULATIONS

In the context of Computational Fluid Dynamics (CFD), lattice Boltzmann methods (LBM) generally refer to explicit numerical schemes that provide asymptotic approximations to the Navier-Stokes equations (NS) at low Mach number $M \ll 1$. Based on a discretization of the BGK approximation of the Boltzmann equation from Kinetic Theory, LBM provides distribution functions on a spacial grid where velocities and pressure fields (that approximate solutions to NS) can be computed through their statistical moments [22].

The BGK-Boltzmann equation models the evolution of the distribution function, f, of a gas of particles. The distribution depends on time, spacial positions, and velocities of the microscopic constituents of the gas. In the present study, numerical simulations were performed using a LBM scheme on a three-dimensional regular Cartesian grid, known as D3Q19. The velocity space is reduced to a set of velocities $\{\vec{e}_i : i = 0, 1, ..., 18\}$ that, from a position in the grid, point to the 18 nearest neighboring nodes, with $e_0 = 0$. The magnitude of these velocities is such that, given a time step δt, $\delta t \vec{e}_i$ represents the position of the ith nearest neighboring node relative to a node in the grid. In this fashion, the distribution function is replaced by a set of 19 distributions $f_i(\vec{x}_j, t)$ that represent f evaluated on the ith velocity and the $\vec{x}_j$ position on the grid at time t.

The time step and the grid spacing can be conveniently set to unity, and the time derivative of f_i can be approximated in a Euler way as a material or Lagrangian derivative, to obtain the discrete version of the BGK-Boltzmann equation:

$$f_i(\vec{x}_j + \vec{e}_i, t + 1) = f_i(\vec{x}_j, t) - 1\tau(f_i(\vec{x}_j, t) - \overline{f}_i(\vec{x}_j, t)). \tag{2}$$

The term with a factor $1/\tau$ is the BGK approximation to the original collision integral of the Boltzmann equation, and τ is the collisional relaxation time, which is associated to the kinetic viscosity of the model fluid

$$\nu = 2\tau - 16. \tag{3}$$

The distribution $\overline{f}_i$ is an approximation of the Maxwell equilibrium function in accordance with the choice of discrete velocities:

$$\overline{f}_i = w_i \rho[1 + 3\vec{e}_i \cdot \vec{v} + 92(\vec{e}_i \cdot \vec{v})^2 - 32\vec{v} \cdot \vec{v}], \tag{4}$$

where w_i are weights of values $w_0 = 1/3$, $w_i = 1/18$ for $i = 1, ..., 6$ and $w_i = 1/36$ for $i = 7, ..., 18$. The equilibrium distribution depends on the macroscopic, or continuum, velocity and density fields ($\vec{v}$ and ρ), computed through the discrete moments:

$$\rho = \sum_{i=0}^{18} f_i \quad \text{and} \quad \rho\vec{v} = \sum_{i=0}^{18} f_i \vec{e}_i. \tag{5}$$

The acoustic pressure is obtained with the equation of state $p = \rho c^2$, where $c = \sqrt{1/3}$.

The computational domain consisted of $301 \times 141 \times 141$ grid nodes. The tube had an interior radius of $R = 20.2$, a thickness of 13.5, and a length of 160 grid lengths, which corresponds to a shorter tube than that used for PIV visualization. Four curvature radii of the mouthpiece where explored, $r = 0, 4.6, 9.2,$ and 13.5 grid lengths. The chosen value of the relaxation time was $\tau = 0.54543$ and the period of oscillation considered was $T = 21\,400$ time steps. Starting from rest ($\vec{v} = \vec{0}$) the simulations took five cycles to reach an oscillatory state. An interpolation scheme of second order for curved surfaces was adopted to impose no-slip boundary conditions on the tube's surface [23]. The open boundaries of the computational domain were modeled with anechoic

boundary conditions, where the unknown distribution functions were determined by a backward linear interpolation [24]. To include the acoustic source inside the tube, we imposed the equilibrium distributions (4) with a sinusoidal varying $\rho(t)$ at its entrance given by

$$\rho(t) = 1 + (0.00013N) \sin(2\pi t/T),\tag{6}$$

where $N = 1, 2, ..., 19$, with $\rho = 1$ initially. Although imposing the value of ρ at the tube entrance using (6) does not guarantee mass conservation over a period of oscillation, it will be shown in the next section that violations of mass conservation are quite small.

To determine the amplitude of the imposed oscillation, measurements were taken at the center of the tube's open end to avoid boundary effects. It should be stressed that we do not expect the LBM to provide quantitative results to match precisely those obtained via PIV, but rather to match qualitatively the main features exhibited by the flow for each value of the dimensionless scaling parameter R_δ.

IV. RESULTS

The setup described in Sec. II A allows for a portrait of the two-dimensional velocity field along the laser sheet to be obtained using phaselocking, with a low frequency of 50 Hz chosen so as to maximize the number of images acquired for each period. We begin by examining the results obtained for the $r = 0$ mm termination, which corresponds to a straight inneredge for the tube. For SPL = 113 dB, where SPL denotes sound pressure level, we have $R_\delta < 1$ and the behavior corresponds to that of a linear system, where the flow structure is symmetric in time, so that inflow and outflow look the same and there is no vortex formation. Three distinct nonlinear regimes are observed, however, and they correspond to increasing values of R_δ, or, equivalently, sound pressure levels, which are obtained after rms-time-averaging the acoustic pressure inside the tube over one oscillation period. Figures 3–5 show images of the tracing particles and the velocity fields and azimuthal components of the vorticity fields obtained both through PIV measurements and LBM simulations at four different phases, and for Reynolds numbers $R_\delta = 20.2, 28.5,$ and $40.2,$ corresponding to SPLs of 140 dB, 143 dB, and 146 dB, respectively. These values have been chosen to illustrate clearly the transition between the three different regimes observed.

Three dimensional numerical simulations allow for validation of the experimental measurements, which was not possible in previous studies employing two-dimensional simulations [3], as they represent flow in a channel and not in a cylindrical tube. For validation purposes we note that there is good qualitative agreement between the PIV measurements and LBM simulations for all three of the aforementioned regimes. The first regime is pictured in Fig. 3 with PIV measurements showing that the outflow-inflow symmetry is already broken and with vorticity being generated just outside the edges of the tube during outflow, where it remains until it then fades away during inflow. This behavior is mirrored closely by the LBM simulation, as expected.

As R_δ increases, more robust vortices form at the open end of the duct and they eventually detach slightly from the inner edge, before being sucked back into the tube, as is shown in Fig. 4, where $R_\delta = 28.5$. Again, the behavior is similar to that described by the LBM simulation, although the vortices in the simulation are very welldefined in comparison to the experimentally-observed structures, which is not surprising, first, because of noise typically associated with the PIV technique itself, and second, because of the fact that very small perturbations that can affect the PIV portrait will not show up in the LBM simulation because of insufficient resolution. For higher acoustic particle velocities we do expect vortex shedding to occur. Indeed, for $R_\delta = 40.2$, vortices form and quickly detach from the inner edge of the tube before traveling in the axial direction with enough strength to persist during inflow, as can be seen in Fig. 5. There is also a noticeably sustained outflow along the axis of the tube. This permanent outflow could be the result of a recirculation of the air inside the box used in the experiments. However, the LBM simulations, which take place in open space, show the same phenomenon occurring, suggesting that at this frequency and this level of acoustic pressure the formation of a jet occurs, and is probably the result of acoustic streaming
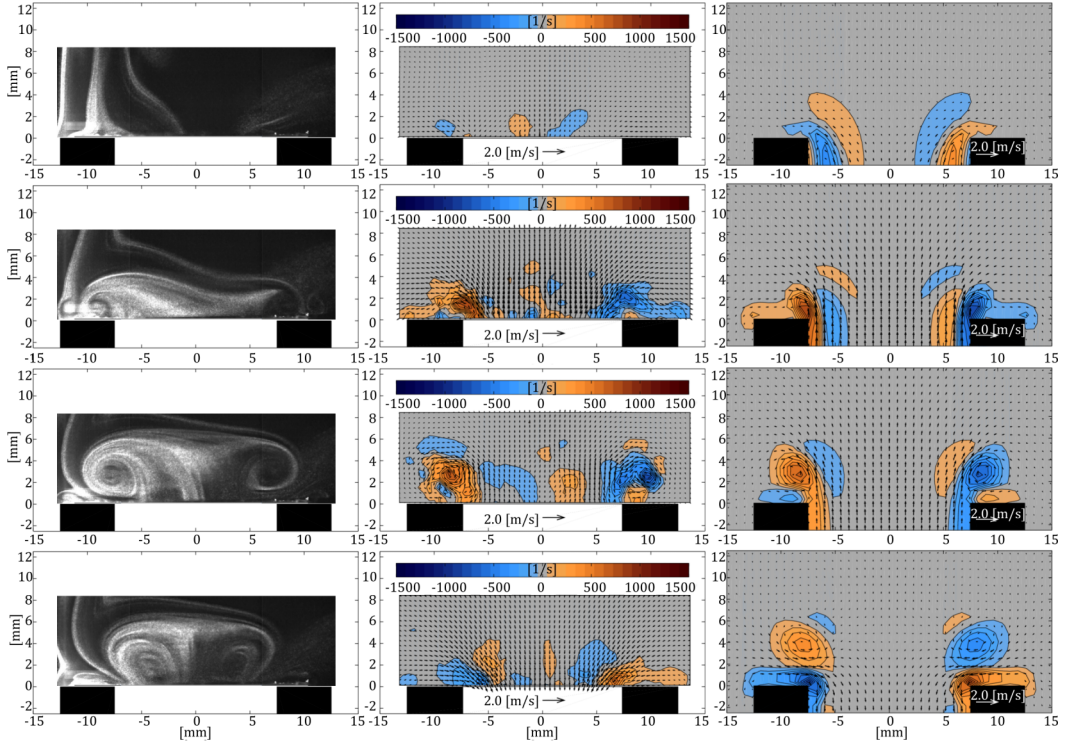
FIG. 4. Nonlinear response at the open end of the duct with $R_\delta = 28.5$ and $r = 0$ mm, where vortices are formed at the open end of the tube. Different plots are organized in the same manner as in Fig. 3.

[25]. Further, to examine this possibility we have used normal-mode decomposition to produce in Fig. 6 a series of scatter plots of the velocity field obtained by means of both PIV and LBM for increasing values of R_δ where we show the values of the zero-frequency mode, which is essentially the mean flow over the whole two-dimensional spatial domain during one period, and of a second normal mode which corresponds to periodic fluctuation amplitudes. These values correspond to the relative magnitudes of a field with mean flow different from zero and a field consisting of periodic perturbations to the mean flow field. The normal modes are identified by means of a Fourier transform in time, which in this case is calculated over thirty five oscillation periods to minimize the effect of noise and random fluctuations. We observe first that for relatively small values of R_δ—see column (a) in Fig. 6—the mean flow is practically nonexistent for both PIV and LBM data, with all points corresponding to the mean flow restricted to a small area close to the origin. However, for larger values of R_δ, mean flow begins to be detectable in both cases in the same region occupied by the fluctuations, indicating increased axial velocity. Finally, for the case $R_\delta = 40.2$, shown in column (c) of Fig. 6, the mean flow extends beyond the region where fluctuations are observed in both the axial and the radial directions. This behavior is more marked for the experimental data than for the numerical simulations, but it is nonetheless clearly observable in both cases. The maximum absolute values of the radial component of the mean flow occur for minimum values of the axial component, and vice versa, suggesting that a pumplike mechanism is feeding the outflow in the axial direction with inflow in the radial direction.

A direct comparison between values of the velocity as measured by PIV and as simulated by LBM is shown in Fig. 7, through the rms-time-averaged volumetric flow over one period of
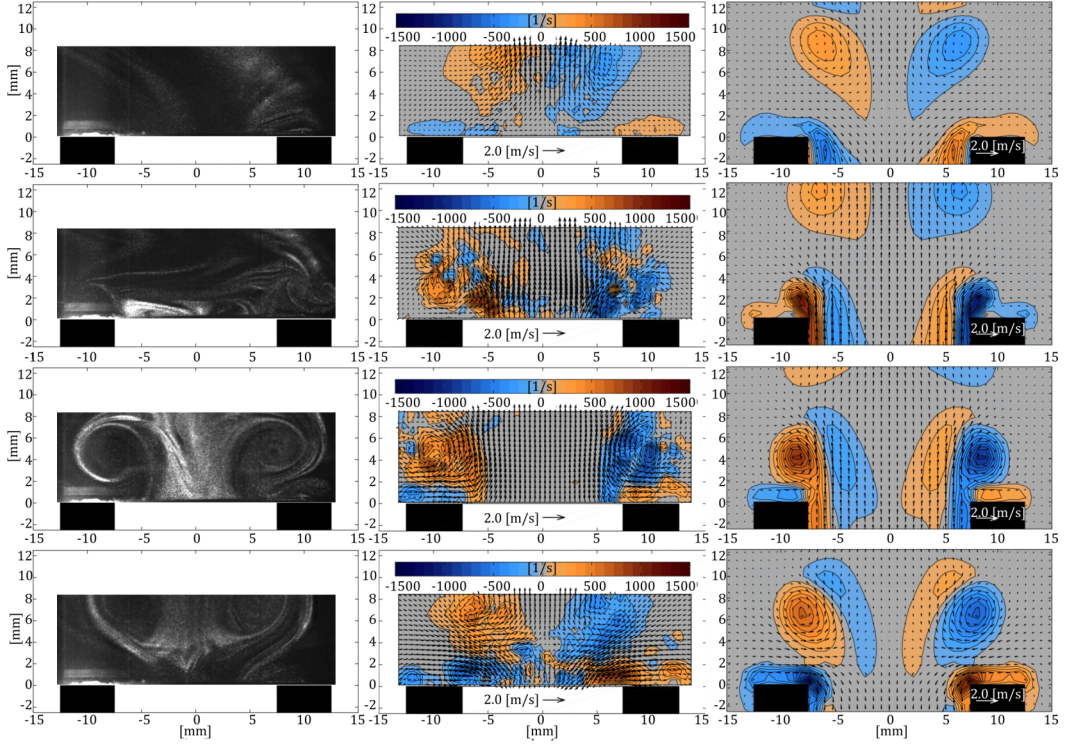
FIG. 5. Nonlinear response at the open end of the duct with $R_\delta = 40.2$ and $r = 0$ mm, illustrating the formation and shedding of vorticity at the inner edge of the open duct. Different plots are organized in the same manner as in Fig. 3.

oscillation:

$$Q = \sqrt{\frac{1}{T} \int_t^{t+T} \left[\int_{\mathcal{S}} \vec{v} \cdot \vec{n} ds \right]^2 d\tau}, \tag{7}$$

where $\mathcal{S}$ represents the tube cross-sectional surface and $\vec{n}$ is a unit vector normal to $\mathcal{S}$ pointing outwards. Figure 7 shows Q computed at the open end of the duct, plotted against the acoustic pressure inside the tube. Velocity was measured 2 mm above the plane defined by the open end of the duct because it was not possible to obtain reliable PIV observations right at the open end, and it was then integrated over the surface of the cross section of the duct to compute Q as a measure of the amplitude of the oscillating flow. The experiment was repeated for twelve different values of R_δ, with correspondingly different values of pressure inside the duct, including the three already examined in Figs. 3–5. Clearly, values of Q increase as R_δ increases, and as this happens experimental data becomes much noisier than numerical data because vortex formation and detachment are not perfectly stable during experiments and local turbulence is produced. As a consequence, values of Q obtained experimentally are somewhat larger than those obtained numerically. With regard to conservation of mass, the inset in Fig. 7 shows the volumetric flow integrated across two cross sections inside the tube ($\mathcal{S}$ taken at the source and at the edge), averaged over 35 cycles, given by

$$\overline{Q} = \frac{1}{35T} \int_0^{35T} \left[\int_{\mathcal{S}} \vec{v} \cdot \vec{n} ds \right] d\tau, \tag{8}$$

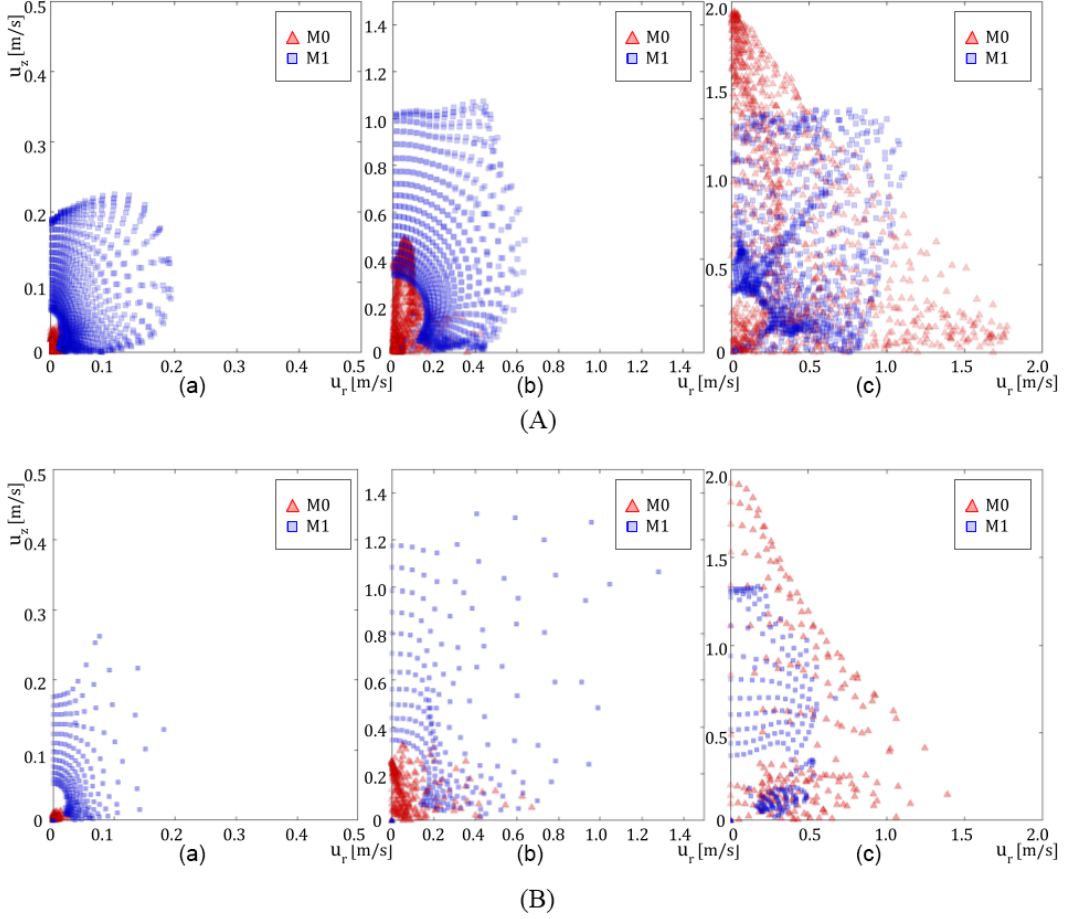relative to Q. It is clearly seen that mass losses are very small.

FIG. 6. Scatter plots obtained through (A) PIV and (B) LBM for the zero-frequency mode (M0) and corresponding fluctuation amplitudes (M1), for $r = 0$ mm and (a) $R_\delta = 8.3$, (b) $R_\delta = 20.2$, and (c) $R_\delta = 40.2$. Plotted points were obtained from velocities calculated over the whole PIV plane of observation and the equivalent plane for the numerical simulations. The axial velocity components u_x are plotted along the vertical axis and the radial velocity components u_r are plotted along the horizontal axis.

It is observed that while the behavior of the experimental and numerical curves is roughly similar, and the scale of the values of mean flow is the same, there is a dip in the curve for the simulated flow slightly below 200 Pa, which corresponds to 140 dB. At this point, vortical structures cease to be destroyed during inflow and persist, as is shown in Fig. 3, and in the case of numerical simulations this results in suddenly decreased amplitude Q through the surface at the exit of the duct, and thus in a sharp dip in the values of Q. For experimental data, this is not clearly appreciated because the noisiness induced by the turbulence offsets the effect of the separation of the vortices. To test this assumption we have treated experimental data using a minimum-order low-pass filter in time so that structures associated with timescales smaller than the period of oscillation are filtered out. After filtering, it is shown in Fig. 7 that experimental measurements of the mean flow match well with the corresponding numerically simulated values. This is not, of course, a rigorous validation of the method, but rather serves to explain the differences observed in the original comparison.

Having checked that the experimental measurements are consistent with the three-dimensional numerical simulations, we use the LBM to produce a portrait of vortex formation and shedding at
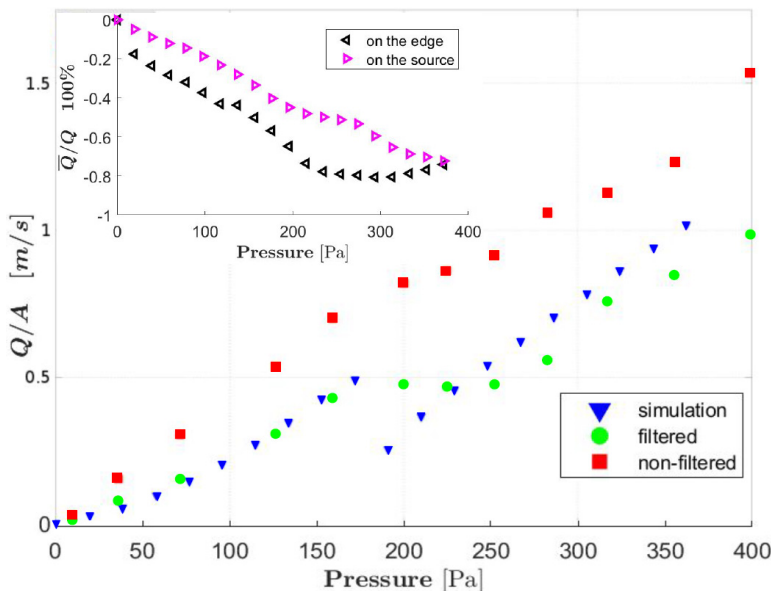
FIG. 7. The amplitude Q just outside the open end of the tube with cross sectional area A plotted against pressure inside the tube for the case $r = 0$ mm. PIV experimental data is depicted by red squares, and LBM numerical data is depicted by blue triangles. Filtered experimental data, where a low-pass filter has been applied which suppresses structures associated with timescales smaller than the period of oscillation, is depicted by green circles. The inset shows the mass conservation properties of the numerical scheme through $\overline{Q}/Q$ measured at the source and at the edge of the tube, plotted against pressure for $r = 0$ mm.

the open end of a tube with $r = 0$, shown in Fig 8. The formation of an annular vortex around the inner edge of the tube can be observed in frames a, b, and c, and the shedding of the vortex is clearly seen in frames d and e. The pumplike mechanism discussed above, which accompanies the outflow, can be clearly appreciated upon examination of the streamlines in this sequence of images.

The effect of rounding the inner edge of the duct is examined by setting $r > 0$ mm. We confirmed previous observations [3] that formation and shedding of vortices are suppressed at the values of R_δ, at which we first observe this phenomenon for $r = 0$ mm, because no separation occurs during inflow because of the rounded edge, which is illustrated in Fig. 1. Nevertheless, we found that it was still possible to observe vortex generation by sufficiently increasing the acoustic pressure inside the tube. At values larger than 150 dB inside the tube, the associated particle velocities become so large—greater than 1.6 m/s—that it is no longer possible to use PIV to calculate them for our particular setup. This is a well-known limitation of the method in particular cases [13,17]. We were still able, however, to obtain qualitative observations of the flow following the motion of tracer particles, which we accompany with the corresponding LBM simulations. In Fig. 9 it is observed that for $R_\delta \approx 26$, vorticity generation at the inner edge of the duct decreases noticeably as the edge becomes more rounded for equal pressure levels inside the duct. Also, note that the behavior shown in the experimental sequences matches that described by the corresponding LBM simulations quite closely. Experimental and numerical sequences also match well in Fig. 10, where the acoustic pressure inside the duct has been greatly increased to give $R_\delta \approx 73$, which is a much larger value than that which corresponds to Fig. 5, for example. In this case vortex shedding does occur for the smaller values of the radius of curvature r, but is eventually suppressed for $r = 5$ mm, as expected. Residual turbulence can be observed for experimental sequences toward the end of an oscillation period, and the velocities associated with this turbulence exceed acoustic particle velocities. It seems that vortex shedding will occur eventually even for large radii of curvature,
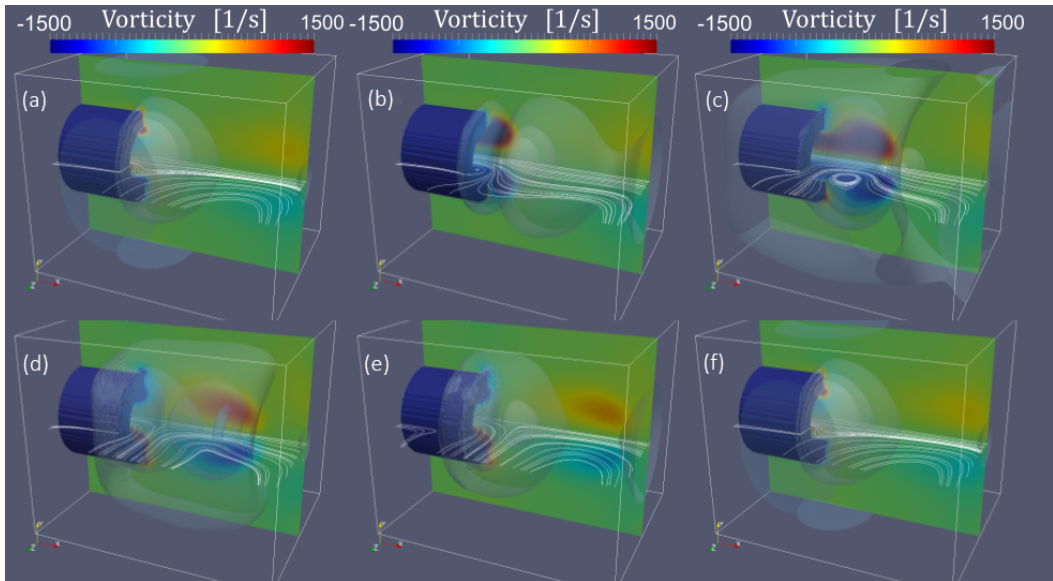
FIG. 8. Formation and shedding of vortices at the open end of the tube for $r = 0$ mm and $R_\delta = 170$. Vorticity is plotted in the xy plane, and streamlines in the xz plane. Surfaces of equal pressure are rendered in white. Phases shown are: (a) $0.0\,T$, (b) $0.2\,T$, (c) $0.4\,T$, (d) $0.6\,T$, (e) $0.8\,T$, and (f) $1.0\,T$, where T is the period of oscillation.

which is not an unforeseen result, as we have established that vortex formation in this case is due to boundary layer separation during inflow, and thus incompressible shear flow, and not to acoustic phenomena.

V. CONCLUSIONS

The generation and shedding of vortices at the inner edge of an open circular duct which contains an acoustic field has been studied using PIV for the experimental calculation of the associated velocity field and LBM for the three-dimensional numerical simulation of the same field, which allows for comparison with the experimental results. Qualitatively, PIV measurements match well with the results of LBM simulations when the inner edge of the tube is straight, but local turbulence accompanies the generation of vorticity during experiments and makes straightforward comparison of velocities impossible. Even so, using a simple high-pass filter to account for small-scale turbulence it was shown that the values of the mean flow calculated experimentally are consistent with those resulting from LBM simulations. This cannot be taken as a formal validation of the Lattice-Boltzmann method, but the method does prove to be adept at representing the transition from acoustical vibration of an air column to the nonlinear dynamics of an inviscid fluid, with velocity fields of the same scale as their experimentally calculated counterparts, notwithstanding the dissipation associated with the method itself [26]. For rounded inner edges of the duct only qualitative comparisons between the visualization of the tracing particles and simulations are possible because of limitations imposed upon the PIV method by the large particle velocities involved. Still, the experimental images also match well against the LBM simulations in these cases, strengthening the claim that the LBM is a robust tool capable of adequately portraying the relevant phenomena.

Our results are consistent with previous work regarding both the existence of different regimes defined by the generation and eventual shedding of vortices at the inner edge of the duct [3] and the effect that rounding this edge has on the aforementioned generation and shedding of vortices [2,4].
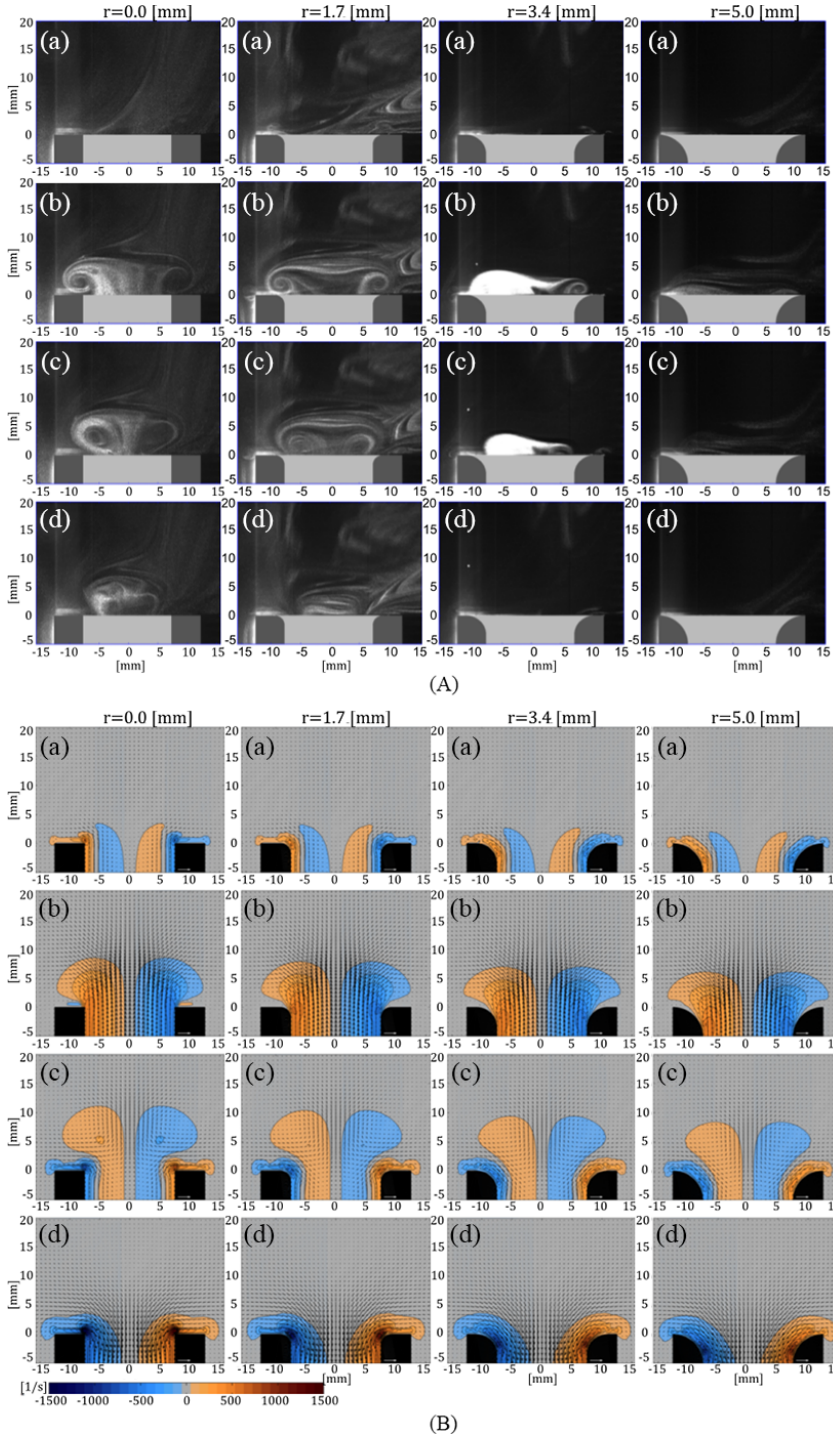
FIG. 9. Flow at the open end of tubes for $R_\delta \approx 26$ with different radii of curvature arranged by columns: $r = 0$ mm, 1.7 mm, 3.4 mm, and 5.0 mm. Shown in different lines are phases $0.0\,T$, $0.3\,T$, $0.5\,T$, and $0.7\,T$ for (A) experiments and (B) the corresponding axial slices of the scaled velocity field and the azimuthal component of the vorticity field $[1/s]$ resulting from the LBM simulations.
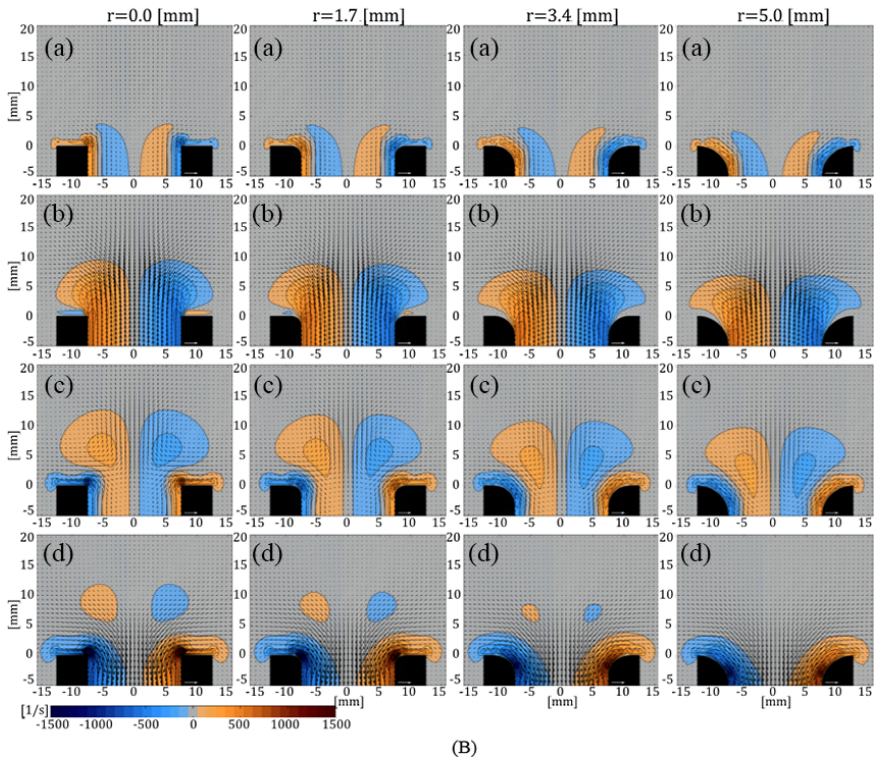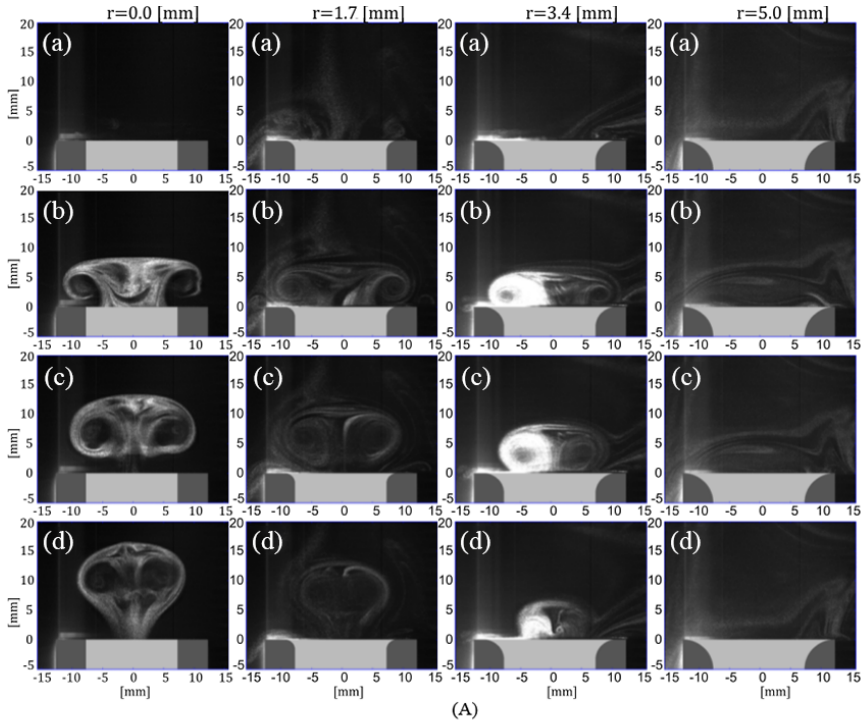
(A)

(B)

FIG. 10. Flow at the open end of tubes for $R_\delta \approx 73$ with different plots organized in the same manner as in Fig. 9.

Three distinct regimes were observed, characterized first by generation of vorticity at the inner edge of the open tube for low particle velocities, then by formation of a well-defined annular vortex at this same location for moderate particle velocities, and finally by shedding of these vortices for high velocities. The actual values of the velocities which are identified with the different regimes were found to depend very strongly on the curvature of the inner edge. The more rounded the edge, the more pressure is needed inside the duct to generate vorticity at the edge. In further studies we will consider horn terminations with different geometries, as it has already been reported that their effect on the aeroacoustic behavior at the open end of the duct can be dramatic. [4].

One aspect of interest to various authors [2,3] has been the quantification of nonlinear losses at the exit of the open tube. It is necessary for this purpose to use three-dimensional simulations, but even then it is far from a straightforward task, mainly, in our view, because of the noisiness introduced by turbulence which is readily apparent in experimental results, but much less pronounced in numerical simulations. Various nonlinear mechanisms are responsible for losses at the exit of the tube, and while vortex formation and shedding is certainly an important one, it is far from the only one. An estimation of these losses is certainly possible using the LBM employed for the present study, but it is unlikely to be reliable with regards to precise values. Nonetheless, a reliable three-dimensional compressible Navier-Stokes portrait of all relevant phenomena at the duct opening, namely, acoustic streaming, viscous boundary-layer separation, generation and shedding of vortices, and radiation of sound, is obtained.

[1] U. Ingård and S. Labate, Acoustic circulation effects and the nonlinear impedance of orifices, J. Acoust. Soc. Am. **22**, 211 (1950).

[2] M. Atig, J. Dalmont, and J. Gilbert, Termination impedance of open-ended cylindrical tubes at high sound pressure level, Comptes Rendus Mécanique **332**, 299 (2004).

[3] J. M. Buick, M. Atig, D. J. Skulina, D. M. Campbell, J. P. Dalmont, and J. Gilbert, Investigation of non-linear acoustic losses at the open end of a tube, J. Acoust. Soc. Am. **129**, 1261 (2011).

[4] M. C. A. M. Peters, A. Hirschberg, A. J. Reijnen, and A. P. J. Wijnands, Damping and reflection coefficient measurements for an open pipe at low mach and low Helmholtz numbers, J. Fluid Mech. **256**, 499 (1993).

[5] A. Chaigne and J. Kergomard, *Acoustics of Musical Instruments* (Springer, New York, 2016).

[6] J. H. M. Disselhorst and L. V. Wijngaarden, Flow in the exit of open pipes during acoustic resonance, J. Fluid Mech. **99**, 293 (1980).

[7] P. Merkli and H. Thomann, Transition to turbulence in oscillating pipe flow, J. Fluid Mech. **68**, 567 (1975).

[8] M. Hino, M. Sawamoto, and S. Takasu, Experiments on transition to turbulence in an oscillatory pipe flow, J. Fluid Mech. **75**, 193 (1976).

[9] J. Peube, Etude expérimentale du champ des vitesses à l'embouchure d'un tuyau sonore excité à de fortes amplitudes (experimentation study of the velocity fields at the open end of a tube excited by high amplitude sound), J. Phys. Colloques **40**, C8-346 (1979).

[10] S. I. Sergeev, Fluid oscillations in pipes at moderate reynolds numbers, Fluid Dyn. **1**, 121 (1966).

[11] C. von Kerczek and S. H. Davis, The stability of oscillatory Stokes layers, Stud. Appl. Math. **51**, 239 (1972).

[12] V. K. Garg, Stability of developing flow in a pipe: non-axisymmetric disturbances, J. Fluid Mech. **110**, 209 (1981).

[13] D. B. Hann and C. A. Greated, The measurement of flow velocity and acoustic particle velocity using particle-image velocimetry, Meas. Sci. Technol. **8**, 1517 (1997).

[14] D. B. Hann and C. Greated, Measurement of acoustic particle velocity using particle image velocimetry techniques, Acustica **83**, 354 (1997).

[15] S. Yoshikawa, H. Tashiro, and Y. Sakamoto, Experimental examination of vortex-sound generation in an organ pipe: A proposal of jet vortex-layer formation model, J. Sound Vib. **331**, 2558 (2012).

[16] J. P. Sharpe, C. Greated, C. Gray, and D. Campbell, Measurement of acoustic streaming using particle image velocimetry, Acustica **68**, 168 (1989).

[17] M. Raffel, C. Willert, S. Wereley, and J. Kompenhans, *Particle Image Velocimetry. A Practical Guide*, 2nd ed. (Springer, 1998).

[18] R. J. Adrian, Particle-imaging techniques for experimental fluid mechanics, Annu. Rev. Fluid Mech. **23**, 261 (1991).

[19] I. Grant, Particle image velocimetry: A review, Proc. Inst. Mech. Eng., Part C **211**, 55 (1997).

[20] D. Skulina, Ph.D. thesis, The University of Edinburgh, 2005.

[21] S. Weyna and W. Mickiewicz, Phase-locked particle image velocimetry visualization of the sound field at the outlet of a circular tube, Acta Phys. Pol. A **125**, A-108 (2014).

[22] S. Chen and G. D. Doolen, Lattice boltzmann method for fluid flows, Annu. Rev. Fluid Mech. **30**, 329 (1998).

[23] Z. Guo, C. Zheng, and B. Shi, An extrapolation method for boundary conditions in lattice Boltzmann method, Phys. Fluids **14**, 2007 (2002).

[24] M. Neal, Ph.D. thesis, The University of Edinburgh, 2002.

[25] J. Lighthill, Acoustic streaming, J. Sound Vib. **61**, 391 (1978).

[26] S. Marié, D. Ricot, and P. Sagaut, Comparison between lattice boltzmann method and Navier–Stokes high order schemes for computational aeroacoustics, J. Comput. Phys. **228**, 1056 (2009).